Energy-Efficient and Environmentally Friendly Solid Oxide Membrane Electrolysis Process for Magnesium Oxide Reduction: Experiment and Modeling

XIAOFEI GUAN, UDAY B. PAL, and ADAM C. POWELL

This paper reports a solid oxide membrane (SOM) electrolysis experiment using an LSM($La_{0.8}Sr_{0.2}MnO_{3-\delta}$)-Inconel inert anode current collector for production of magnesium and oxygen directly from magnesium oxide at 1423 K (1150 °C). The electrochemical performance of the SOM cell was evaluated by means of various electrochemical techniques including electrochemical impedance spectroscopy, potentiodynamic scan, and electrolysis. Electronic transference numbers of the flux were measured to assess the magnesium dissolution in the flux during SOM electrolysis. The effects of magnesium solubility in the flux on the current efficiency and the SOM stability during electrolysis are discussed. An inverse correlation between the electronic transference number of the flux and the current efficiency of the SOM electrolysis was observed. Based on the experimental results, a new equivalent circuit of the SOM electrolysis process is presented. A general electrochemical polarization model of SOM process for magnesium and oxygen gas production is developed, and the maximum allowable applied potential to avoid zirconia dissociation is calculated as well. The modeling results suggest that a high electronic resistance of the flux and a relatively low electronic resistance of SOM are required to achieve membrane stability, high current efficiency, and high production rates of magnesium and oxygen.

I. INTRODUCTION

SOLID oxide membrane (SOM) electrolysis is an electrolytic metal extraction technique that is low in energy and capital costs, and also environmentally friendly. It requires minimum preprocessing, the plant is scalable, and has a smaller footprint. The process directly reduces oxides or oxide compounds to their respective metals, alloys, or intermetallics, such as magnesium (Mg), tantalum (Ta), titanium (Ti), calcium (Ca), ytterbium (Yb), silicon (Si), Ti-Fe alloy, Ti-Si intermetallics, *etc*.[1–17]

Because of its simplicity and efficiency, the SOM process is the lowest-cost method proposed for producing Mg with cost estimated at $1.36/kg, much lower than that for $MgCl_2$ electrolysis, siliconthermic reduction (the Pidgeon process), and the carbothermic reduction.[7] The SOM process for Mg production employs an oxygen-ion-conducting yttria-stabilized zirconia (YSZ) membrane to separate a liquid metal anode from a molten fluoride flux containing magnesium oxide (MgO). During electrolysis, magnesium cations are reduced at the cathode, while oxygen anions are transported through the YSZ membrane to the anode where they are oxidized. It has been reported that a novel LSM ($La_{0.8}Sr_{0.2}MnO_{3-\delta}$)-Inconel inert anodic current collector and liquid silver anode are successfully used in SOM electrolysis experiments for O_2 evolution.[6] The YSZ membrane selectively conducts oxygen ions but blocks other elements such as fluorine. In addition, the YSZ membrane prevents O_2 from back-reaction with the reduced Mg. Therefore, the pure O_2 evolved can be easily collected and also sold to offset some of the capital cost and further lower the Mg price point.

Previous work has shown that Mg has a finite solubility in the fluoride flux used in SOM electrolysis.[4–6,18,19] The dissolution of Mg imparts electronic conductivity to the flux, which negatively affects the SOM electrolysis in two ways: First, the electronic conductivity of the flux decreases the SOM electrolysis current efficiency. SOM electrolysis has been shown to have high current efficiencies (approximately 90 pct) at the beginning for short time periods.[2,18] However, as the electrolysis continues, the current efficiency drops significantly to 40 through 50 pct due to electronic current in the flux caused by the dissolved Mg.[4,18] Second, the electronic conductivity in the flux provides a pathway for the applied potential to reduce the zirconia (ZrO_2) at the outer surface of the YSZ membrane.[20] YSZ membrane is known to be stable in MgF_2-CaF_2 flux containing a small concentration of YF_3, when no electric potential is applied across the membrane.[21]

XIAOFEI GUAN, Postdoctoral Research Associate, and UDAY B. PAL, Professor, are with the Department of Mechanical Engineering and the Division of Materials Science and Engineering, Boston University, Boston, MA. Contact e-mail: upal@bu.edu ADAM C. POWELL, Chief Technology Officer, is with Infinium Inc., Natick, MA.

However, when the flux has some electronic conductivity, it is possible for the flux to essentially act as an extended cathode. In this case, the applied potential reduces the ZrO$_2$ at the surface of the YSZ membrane. Gratz et al.[20] have observed the YSZ membrane degradation due to the electrochemical dissociation of ZrO$_2$ during SOM electrolysis.

Regarding the important role of Mg solubility, it is important to monitor and evaluate Mg dissolution in the flux during electrolysis. In this work, electronic transference numbers of the flux ($t_{e,flux}$) between two steel electrodes are measured to assess the Mg dissolution in the flux during electrolysis. The correlation between $t_{e,flux}$ and the current efficiency of the SOM electrolysis is discussed. Based on the electrochemical characterizations, a new equivalent circuit is presented to model the SOM electrolysis process. In addition, a polarization model of SOM process for Mg and O$_2$ production is developed, and the maximum allowable applied potential to avoid ZrO$_2$ dissociation is calculated. Modeling of the SOM electrolysis process provides insights for increasing both the current efficiency and the YSZ membrane stability.

II. EXPERIMENTAL

A. SOM Electrolysis Setup

Figure 1 shows the schematic of a SOM electrolysis setup. It consisted of an upper reaction chamber heated to 1423 K (1150 °C) and a lower condensing chamber having a temperature gradient of 1373 K to 473 K (1100 °C to 200 °C). The setup was fabricated using grade 304 stainless steel (SS-304) and heated in industrial grade Ar (Airgas). Inside the reaction chamber, 470 g of powdered flux (45 wt pct MgF$_2$-55 wt pct CaF$_2$ containing 5 wt pct MgO and 2 wt pct YF$_3$) was used to form the molten electrolyte; 45 wt pct MgF$_2$-55 wt pct CaF$_2$ is a eutectic composition having a melting temperature of 1247 K (974 °C)[22]; YF3 was added to prevent yttrium depletion from the YSZ membrane.[21] A one-end-closed 6 mol pct YSZ tube (McDanel Advanced Ceramics) separated the flux from 44 g of liquid silver encased inside the YSZ tube. An LSM-Inconel inert anode current collector was disposed in the YSZ tube and was submerged in the liquid silver anode.[23] An SS-304 bubbling tube served as the cathode. Alumina spacers were used to electrically isolate the YSZ membrane and the bubbling tube from the reaction chamber.

During the experiment, forming gas (95 pct Ar-5 pct H$_2$) was used to purge the reaction chamber. The gas flowing rate through the bubbling tube was 180 cm^3/min, and the flow rate through the annulus between the bubbling tube and the SS-304 tube extending out of the top of the reaction chamber was 300 cm^3/min. There was no gas flow through the annulus between the YSZ membrane and its outside SS-304 tube. The forming gas lowered the partial pressure of Mg vapor over the flux and carried the Mg vapor into the condenser (see Figure 1). The Mg vapor in the condenser was cooled and condensed on a steel shim placed along the inner walls of the chamber. The bubbling gas also stirred the flux to facilitate the transport of Mg vapor out of the flux and achieve chemical homogeneity in the flux.

1. Electrochemical characterization of SOM electrolysis cell

The electrochemical characterization of the SOM electrolysis cell was performed between the LSM-Inconel inert anode current collector and the bubbling tube cathode. Electrochemical impedance spectroscopy (EIS) scans were performed to measure the ohmic resistance of the SOM electrolysis cell. The EIS scans were performed using a Princeton Applied Research 263A potentiostat and a Solartron 1250 frequency response analyzer. These impedance scans were from 20,000 to 1 Hz with 20 mV amplitude. The ohmic resistance of the measured cell was obtained from the value of the high-frequency intercept on the real axis of the Nyquist plot.[24,25]

When an applied potential exceeded the dissociation potential of MgO, Mg vapor was produced at the bubbling tube cathode, and O$_2$ evolved at the liquid silver anode. The overall cell reaction is given as

$$MgO = Mg(g) + \frac{1}{2}O_2(g) \qquad [1]$$
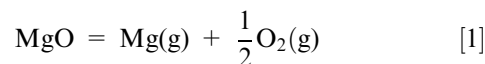
Potentiodynamic scans at 5 mV/s were performed to determine the dissociation potential of MgO. Electrolysis runs were performed by applying a constant electric potential greater than the dissociation potential of MgO. The potentiodynamic scans and the electrolysis runs were performed using an Agilent Technologies N5743A power source. O$_2$ gas evolution was observed at the anode once the liquid silver anode became saturated with O$_2$. The anode exit gas passed through a FMA-4305 digital flow meter (OMEGA Engineering) that measured the flow rate of the evolved O$_2$.

2. Measurement of the electronic transference number of the flux

Periodically, the electrolysis was halted, and the electronic transference number of the flux between the reaction chamber and the bubbling tube was measured to assess the Mg dissolution in the flux. The electronic and ionic resistances of the flux can be modeled by two resistors in parallel. Therefore, the relationship between the total ohmic resistance ($R_{T(flux)}$), the ohmic electronic resistance ($R_{e(flux)}$), and the ohmic ionic resistance ($R_{i(flux)}$) of the flux between the reaction chamber anode and the bubbling tube cathode can be expressed by

$$\frac{1}{R_{T(flux)}} = \frac{1}{R_{e(flux)}} + \frac{1}{R_{i(flux)}} \qquad [2]$$

EIS scan was performed between the reaction chamber and the bubbling tube to determine $R_{T(flux)}$, and it was equal to the value of the high–frequency intercept on the real axis of the Nyquist plot. The ohmic electronic resistance, $R_{e(flux)}$, was determined by performing a
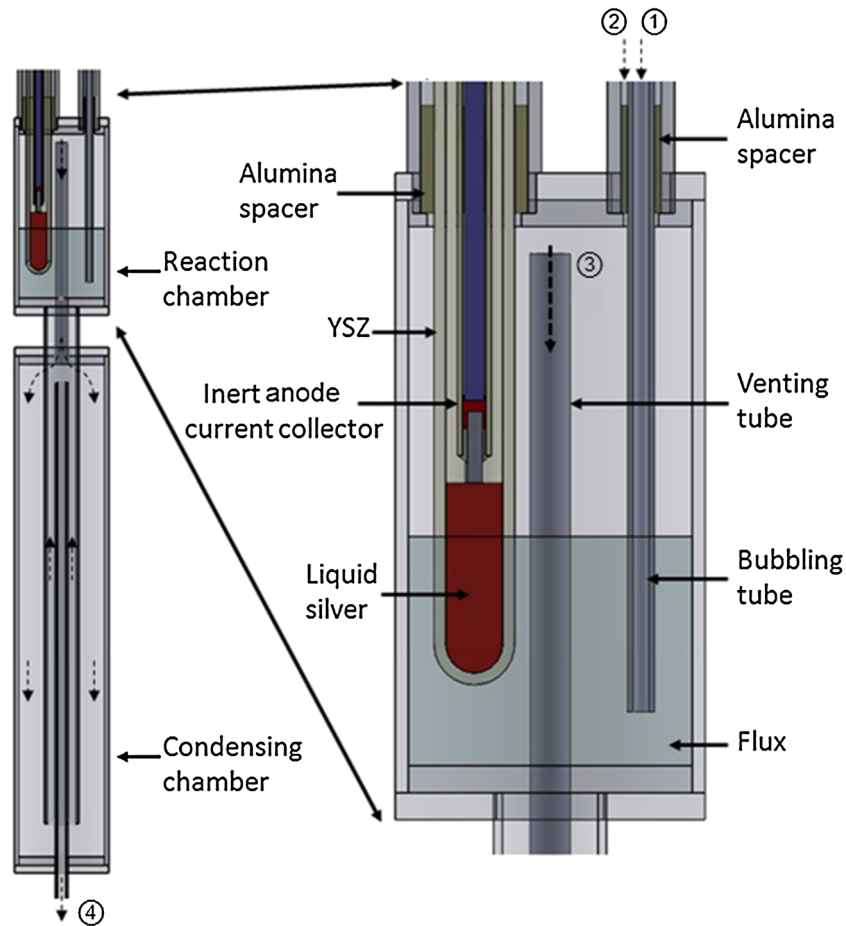
Fig. 1—Schematic of the cross section of a SOM electrolysis setup. The components of the setup are indicated by the solid arrows. The dashed arrows show the flow of forming gas: 1 forming gas flowing through the bubbling tube into the reaction chamber, 2 forming gas flowing through the annulus between the bubbling tube and its outside SS-304 tube, 3 forming gas and Mg vapor mixture flowing through the venting tube leading to the condensing chamber, and 4 forming gas flowing out.

potentiostatic hold between the two electrodes using a Princeton Applied Research 263A potentiostat. In each potentiostatic hold, a constant electric potential (~0.1 V) is applied, and the current response was measured. The ohmic electronic resistance, $R_{e(flux)}$, was obtained by dividing the applied potential by the measured current. It should be noted that the anodic terminal was switched from the liquid silver to the reaction chamber for the above EIS and the potentiostatic holds.

According to Eq. [2], $R_{i(flux)}$ was calculated from the measured values of $R_{T(flux)}$ and $R_{e(flux)}$. Based on the knowledge of $R_{e(flux)}$ and $R_{i(flux)}$, $t_{e(flux)}$ was calculated using the following equation[26]:

$$t_{e(flux)} = \frac{R_{i(flux)}}{R_{e(flux)} + R_{i(flux)}} \quad [3]$$

3. Microstructural characterization

After the SOM electrolysis experiment, the setup was disassembled for detailed analysis and characterization. A piece of the YSZ membrane was mounted in epoxy, polished, coated with gold, and then examined using a JSM-6100 JEOL scanning electron microscope (SEM).

III. RESULTS

A. Ohmic Resistance of the SOM Cell

At the beginning of the experiment, an EIS scan was performed between the inert anode current collector and the bubbling tube, and the results are shown in Figure 2. The high–frequency intercept on the Nyquist plot corresponds to the cell ohmic resistance, which includes the resistances of the YSZ membrane, the flux, the electrodes, the external lead wires, and the contact resistances associated with all the interfaces. The cell ohmic resistance was measured to be 0.54 Ω, close to earlier reported SOM electrolysis cell resistance obtained with LSM-Inconel current collector.[6]

B. Current–Potential Characteristics of the SOM Cell

A PDS was conducted between the inert anode current collector and the bubbling tube after the EIS, and the current–potential relationship is shown in Figure 3. The dissociation potentials of the impurity oxides (such as Fe_2O_3 dissolved into the flux from the crucible walls) and MgO were identified to be approximately 1.3 V and 2.17 V, respectively. The leakage
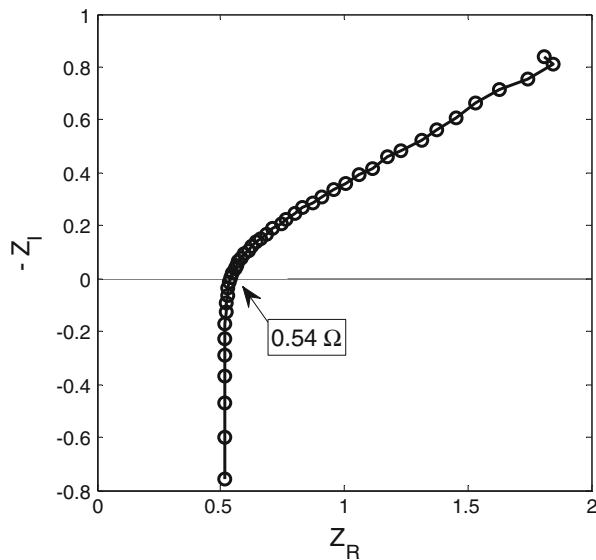
Fig. 2—Electrochemical impedance spectroscopy (EIS) results at the beginning of the SOM electrolysis experiment at 1423 K (1150 °C). The ohmic resistance of the SOM cell was 0.54 Ω.
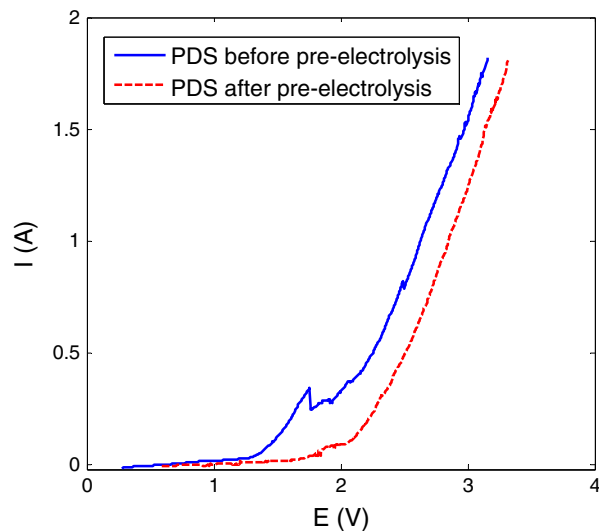

Fig. 3—Potentiodynamic scans (5 mV/s) showing the current–potential relationships before pre-electrolysis (solid line) and after pre-electrolysis (dashed line).

current caused by the dissociation of impurity oxides is approximately 0.4 A. To reduce the leakage current, a pre-electrolysis at an electric potential slightly less than 2.17 V was performed to dissociate the impurity oxides. The starting current was measured to be 0.484 A. After 70 minutes of pre-electrolysis, the measured current dropped to a negligibly small value (0.022 A), and then the pre-electrolysis was stopped. The total charge passed during pre-electrolysis was 289 C.

After the pre-electrolysis, another PDS was conducted between the LSM-Inconel inert anode current collector and the bubbling tube, and the current–potential relationship is also shown in Figure 3. The leakage current caused by impurity oxides was significantly reduced by

the pre-electrolysis. The negligible leakage current also indicates that there was no electronic current since no Mg was generated and dissolved in the flux during pre-electrolysis. The electric potential for MgO dissociation was identified to be approximately 2.08 V. At this point of time, the impurity oxides had been removed, and there was no dissolution of Mg in the flux yet.

C. SOM Electrolysis Runs

Afterward, electrolysis was performed thrice, each for 6 hours, between 2.3 and 2.6 V, to dissociate MgO (see Figure 4). During electrolysis, the O_2 gas produced at the anode passed through a digital flow meter that measured the O_2 evolution rate. The current efficiency is calculated by dividing the faradaic current for O_2 production by the total current passing through the cell. The calculated current efficiency is shown in Figure 5. The steady-state current efficiency decreased as more Mg was produced during SOM electrolysis.

D. Electronic Transference Number of the Flux

Before the first electrolysis, and immediately after each electrolysis, $t_{e(flux)}$ between the bubbling tube and the reaction chamber were measured. The dependence of $t_{e(flux)}$ as a function of time is shown in Figure 5, and the values are listed in Table I. It is shown in Figure 5 that initially $t_{e(flux)}$ was low and the current efficiency was high, but with continued electrolysis the efficiency decreased and $t_{e(flux)}$ increased until the flux reached the solubility limit for Mg dissolution. This indicates an inverse correlation between the current efficiency of the SOM electrolysis and the electronic conductivity of the flux.

E. Post-Experimental Analysis

After the SOM electrolysis experiment, the furnace was cooled, and the setup was disassembled. Figure 6 shows the Mg collected on the stainless steel shim lining the inner walls of the condenser. Figure 7 shows the SEM images of a piece of the YSZ membrane sample. The outer layer of the YSZ membrane contacting the flux showed high porosity. This indicates that the YSZ membrane's degradation took place during the electrolysis. This result is consistent with what has been observed in previous work.[20]

IV. MODELING

A. Equivalent Circuit Modeling

Equivalent circuit is a very useful tool to model the SOM electrolysis process for producing Mg and O_2. Based on the experimental results, it is now understood that the impurity oxides (such as Fe_2O_3) in the flux contribute to the leakage current. It is also known that the dissolved Mg in the flux imparts electronic conductivity to the flux. The electronic conductivity in the flux reduces the current efficiency of the SOM electrolysis and provides a pathway for the applied potential to

dissociate ZrO_2 in the YSZ membrane. A new equivalent circuit of the SOM electrolysis process is presented as shown in Figure 8. The symbols used in Figure 8 are defined in Table II. This equivalent circuit is more comprehensive than those presented by Krishnan et al.[2] and Gratz et al.,[20] because it takes into account (1) the

dissociation of Fe_2O_3 dissolved in the flux, (2) the electronic conductivity of the flux caused by dissolved Mg, and (3) the dissociation of ZrO_2 in the YSZ membrane.

The equivalent circuit first shows that impurity oxides, such as Fe_2O_3, with greater cation electronegativity than Mg will dissociate before MgO. A pre-electrolysis is usually conducted to remove the Fe_2O_3.

After the pre-electrolysis, an electric potential exceeding the dissociation potential of MgO is applied. Once the MgO dissociates, Mg is produced at the cathode. Some of the Mg produced dissolves in the flux, and the rest evolves as vapor and is carried away by the forming gas or argon. The dissolved Mg subsequently increases the electronic conductivity of the flux. The YSZ membrane has electronic conductivity at the operating temperature [1423 K (1150 °C)] and the other prevailing experimental conditions.[27] A flux with electronic conductivity essentially serves as an extended cathode, and it allows electronic current to pass through the flux and the membrane, decreasing the current efficiency. If the flux had no electronic conductivity, then the current passing through the flux would be purely ionic, and the entire energy input to the cell would be used in the process of dissociating MgO. The presence of an electronic current acts as an internal short circuit in the SOM process.
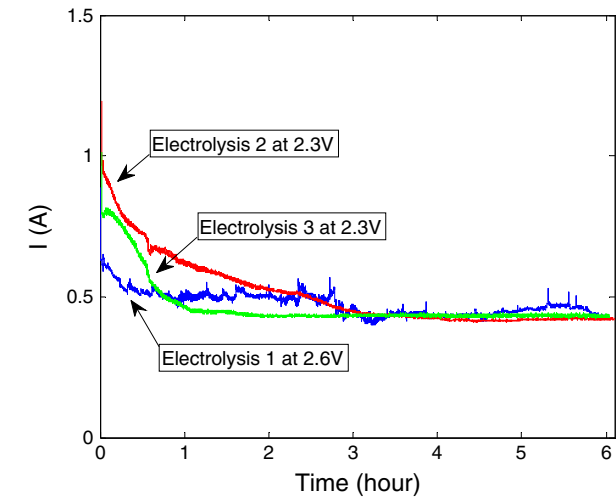

Fig. 4—The current–time plots during the three electrolyses at 1423 K (1150 °C) with applied potentials between 2.3 and 2.6 V.
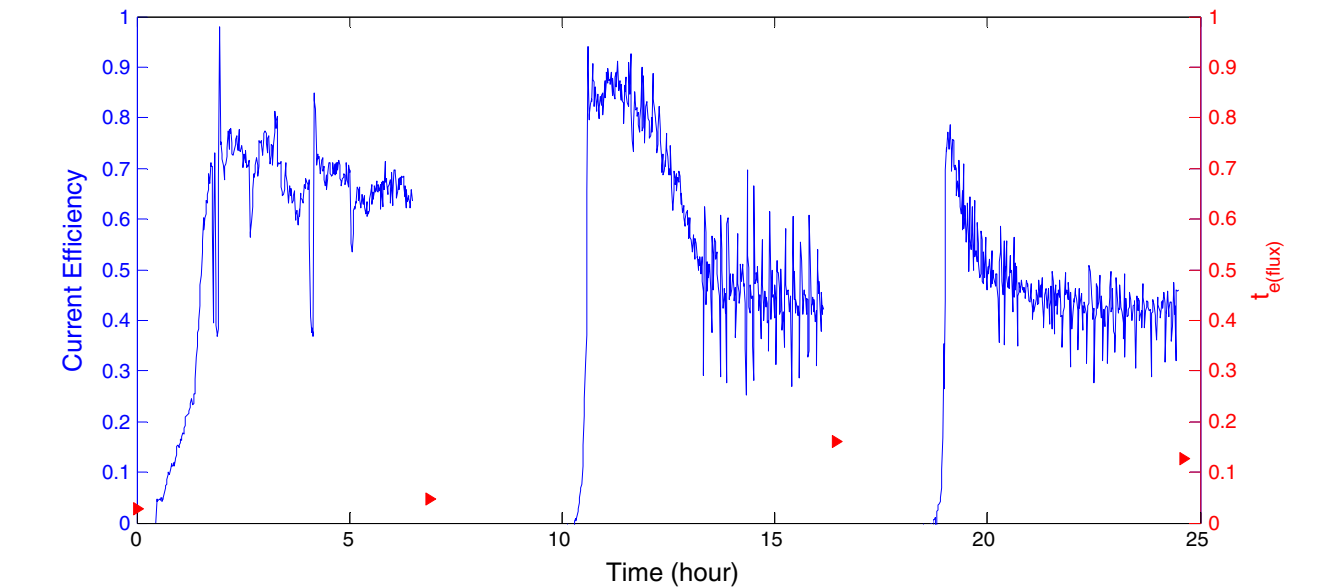

Fig. 5—The decrease in the current efficiency (solid line) during electrolysis as the Mg dissolves in the flux and the electronic transference number (red triangle) increases. The asymptotic behavior indicates that the flux reaches the solubility limit for Mg dissolution (Color figure online).

Table I. The Measured Resistances ($R_{T(flux)}$, $R_{e(flux)}$, and $R_{i(flux)}$) and the Electronic Transference Number ($t_{e(flux)}$) of the Flux Between the Reaction Chamber and the Bubbling Tube

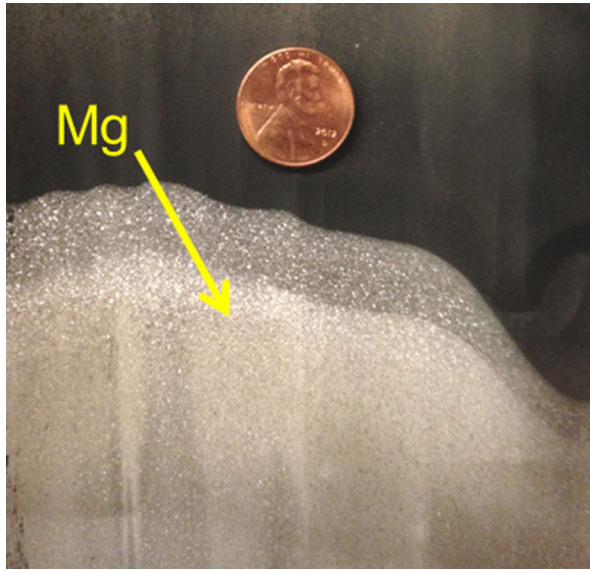| Measurement	$R_{T(flux)}$ (Ω)	$R_{e(flux)}$ (Ω)	$R_{i(flux)}$ (Ω)	$t_{e(flux)}$
1st	0.160	5.857	0.164	0.027
2nd	0.150	3.110	0.158	0.048
3rd	0.168	1.048	0.200	0.160
4th	0.126	1.001	0.144	0.126

Fig. 6—Mg collected on the stainless steel shim lining the inner walls of the condenser shown in scale with a US one-cent coin.

As more Mg dissolves into the flux, the electronic conductivity of the flux will further increase. The increased electronic conductivity also decreases the electronic potential drop across the flux, and then the potential drop across the YSZ membrane must correspondingly increase, while a constant DC electric potential is applied across the entire cell. The increased potential drop across the YSZ can cause the dissociation of ZrO_2, which will degrade the YSZ membrane. To avoid ZrO_2 dissociation, the potential drop across the YSZ membrane should not exceed the dissociation potential of ZrO_2.

B. Polarization Model for Mg and O_2 production

After the Fe_2O_3 is removed and before any Mg is dissolved in the flux, the electronic resistance of the flux is very high; therefore it is reasonable to assume that the entire current is used for dissociating MgO during electrolysis. In this case, only the circuit branch for MgO dissociation needs to be considered, and the remaining branches can be ignored (see the equivalent circuit in Figure 8. The applied potential ($E_{applied}$) can be expressed as follows:

$$E_{applied} = \left| E_N^{MgO} \right| + \eta_{ohm} + \eta_{act} + \eta_{conc,c} + \eta_{conc,a} + \eta_{over,anode/YSZ}, \quad [4]$$

where $\left| E_N^{MgO} \right|$ is the absolute value of the Nernst potential for MgO dissociation, η_{ohm} is the ohmic polarization of the SOM electrolysis cell, η_{act} is the activation polarization, $\eta_{conc,c}$ is the cathodic concentration polarization, $\eta_{conc,a}$ is the anodic concentration polarization, and $\eta_{over,anode/YSZ}$ is the overpotential for oxygen gas evolution at the anode/YSZ interface.

1. Nernst potential for MgO dissociation, E_N^{MgO}

When the Mg produced nucleates in the gaseous state, the Nernst potential for MgO dissociation is given by Eq. [5], where $E_N^{0,MgO}$ is the standard Nernst potential for MgO

dissociation (2.31 V),[6] R is the gas constant (8.31 J/(mol·K)), T is the operating temperature [1423 K (1150 °C)], F is the Faraday constant (96485 C/mol), $a_{MgO(flux)}$ is the activity of MgO dissolved in the flux, $a_{Mg(g),c}$ is the activity of Mg vapor near the cathode, and $a_{O_2(g),anode/YSZ}$ is the activity of the evolved O_2 at the liquid silver/YSZ interface. During SOM experiment, $|E_N^{MgO}|$ was identified at the deflection point of the current–potential curve obtained from PDS between the inert anode current collector and the bubbling tube cathode.

$$E_N^{MgO} = E_N^{0,MgO} + \frac{RT}{2F} \ln \left[\frac{a_{MgO(flux)}}{a_{Mg(g),c} \cdot \left(a_{O_2(g),anode/YSZ} \right)^{\frac{1}{2}}} \right] \quad [5]$$

2. Ohmic polarization, η_{ohm}

The ohmic polarization (η_{ohm}) of the SOM electrolysis cell could be expressed as follows:

$$\eta_{ohm} = iR_{ohm}, \quad [6]$$

where i is the cell current, and R_{ohm} is the ohmic resistance of the SOM electrolysis cell. R_{ohm} can be measured by EIS between the inert anode current collector and the bubbling tube cathode.

3. Activation polarization, η_{act}

The additional potential needed to overcome the activation energy barrier for the charge transfer reactions at the electrode/electrolyte interface is called activation polarization, η_{act}. For small currents and/or rapid mass transfer, it is related to the cell current i by the following Butler–Volmer equation[28–30]:

$$i = i_0 \exp \left(\frac{\alpha n \eta_{act} F}{RT} \right) - i_0 \exp \left(\frac{-(1-\alpha) n \eta_{act} F}{RT} \right), \quad [7]$$

where i_0 is the exchange current, α is the transfer coefficient, and $n = 2$ is the number of electrons transferred. Both activation polarizations occurring at the anode and the cathode are lumped together in η_{act}. The exchange current i_0 is a measure of the electrocatalytic activity of the electrode/electrolyte interface for a given electrochemical reaction, and it depends on the operating conditions and materials properties. The transfer coefficient for SOM electrolysis cell is suggested to be 0.5 assuming a symmetric activation energy barrier for both electrode reactions. Then, Eq. [7] can be solved for η_{act} as a function of i:

$$\eta_{act} = \frac{RT}{F} \ln \left[\left(\frac{i}{2i_0} \right) + \sqrt{\left(\frac{i}{2i_0} \right)^2 + 1} \right] \quad [8]$$

4. Cathodic concentration polarization, $\eta_{conc,c}$

The cathodic concentration polarization $\eta_{conc,c}$ is caused by the mass transport of MgO across the diffusion layer at the cathode surface and can be expressed as follows[30]:
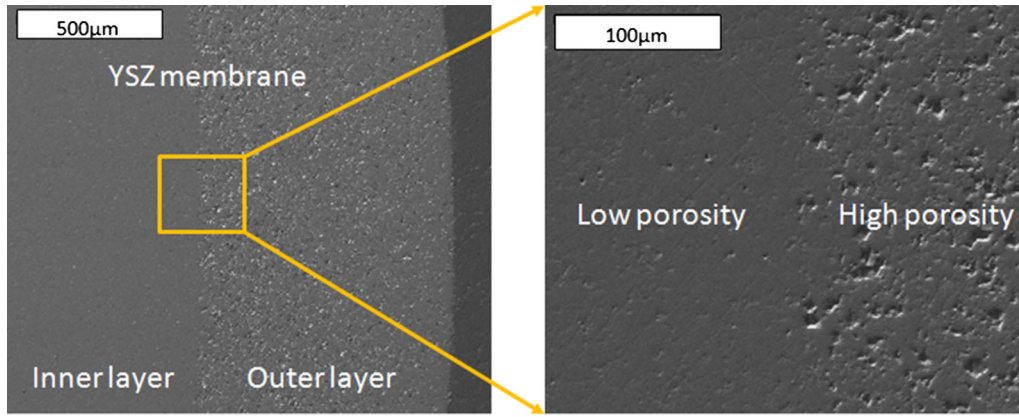
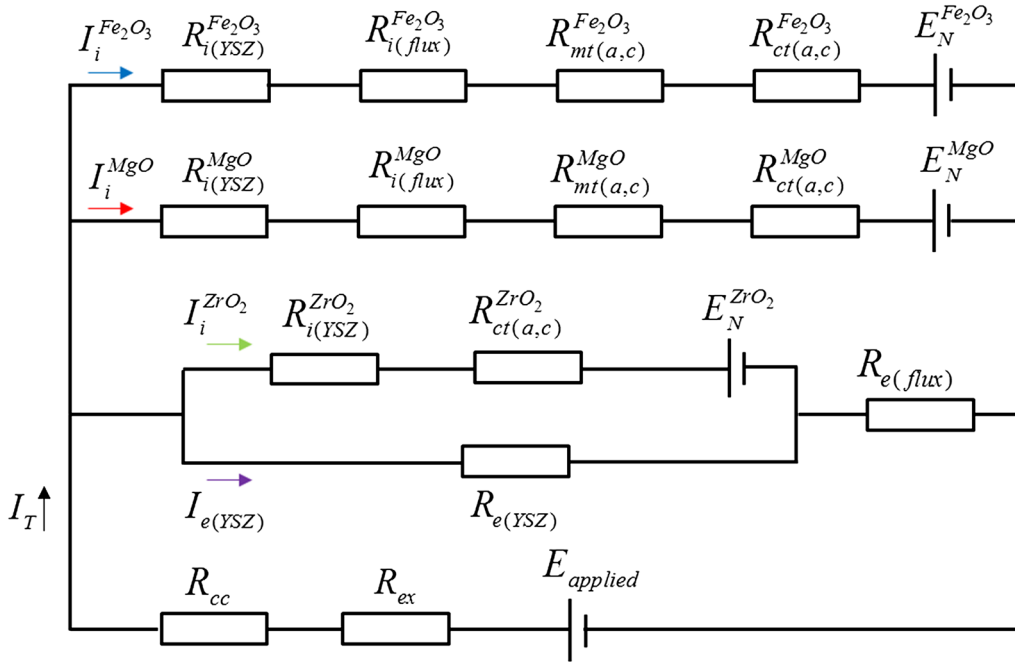Fig. 7—SEM images of the membrane cross section after the SOM electrolysis.

Fig. 8—Equivalent circuit of the SOM electrolysis process for magnesium and oxygen production.

$$\eta_{\text{conc,c}} = \frac{RT}{2F} \ln\left(\frac{a^0_{\text{MgO(flux)}}}{a^{(i)}_{\text{MgO(flux)}}}\right), \quad [9]$$

where $a^0_{\text{MgO(flux)}}$ is the activity of MgO in the bulk flux, and $a^{(i)}_{\text{MgO(flux)}}$ is the activity of MgO at the flux/cathode interface under a certain current density. Assuming a Henrian solution, Eq. [9] can be written as follows:

$$\eta_{\text{conc,c}} = \frac{RT}{2F} \ln\left(\frac{C^0_{\text{MgO(flux)}}}{C^{(i)}_{\text{MgO(flux)}}}\right), \quad [10]$$

where $C^0_{\text{MgO(flux)}}$ and $C^{(i)}_{\text{MgO(flux)}}$ are the concentrations of MgO in the bulk flux and at the flux/cathode interface, respectively.

The concentration gradient drives the diffusion of MgO at the cathodic surface. Assuming a linear concentration gradient within the diffusion layer, the diffusive flux of MgO at the cathodic surface can be expressed by Fick's first law as follows:

$$J_{\text{MgO,flux/cathode}} = -D_{\text{MgO(flux)}} \frac{dC_{\text{MgO(flux)}}}{dx} = $$
$$-D_{\text{MgO(flux)}} \frac{C^{(i)}_{\text{MgO(flux)}} - C^0_{\text{MgO(flux)}}}{\delta_c} \quad [11]$$

where $D_{\text{MgO(flux)}}$ is the diffusion coefficient of MgO in the flux, and δ_c is the thickness of the diffusion layer at the cathode surface.

Relating the diffusive flux of MgO, $J_{\text{MgO,flux/cathode}}$, to the cell current, i, gives

Table II. Definitions of Symbols in the SOM Equivalent Circuit Shown in Fig. 8

Symbol	Definition	Symbol	Definition
$R_{i(YSZ)}^{Fe_2O_3}$	ionic resistance of YSZ membrane involved for Fe$_2$O$_3$ dissociation	R_{cc}	resistance of the inert anode current collector
$R_{i(YSZ)}^{MgO}$	ionic resistance of YSZ membrane involved for MgO dissociation	R_{ex}	resistance of external lead wires
$R_{i(YSZ)}^{ZrO_2}$	ionic resistance of YSZ membrane involved for ZrO$_2$ dissociation	$E_N^{Fe_2O_3}$	Nernst potential for Fe$_2$O$_3$ dissociation
$R_{i(flux)}^{Fe_2O_3}$	ionic resistance of flux (between YSZ and bubbling tube) involved for Fe$_2$O$_3$ dissociation	E_N^{MgO}	Nernst potential for MgO dissociation
$R_{i(flux)}^{MgO}$	ionic resistance of flux (between YSZ and bubbling tube) involved for MgO dissociation	$E_N^{ZrO_2}$	Nernst potential for ZrO$_2$ dissociation
$R_{mt(a,c)}^{Fe_2O_3}$	mass transfer resistance at the anode and cathode for Fe$_2$O$_3$ dissociation	$E_{applied}$	applied potential
$R_{mt(a,c)}^{MgO}$	mass transfer resistance at the anode and cathode for MgO dissociation	$I_i^{Fe_2O_3}$	ionic current for Fe$_2$O$_3$ dissociation
$R_{ct(a,c)}^{Fe_2O_3}$	charge transfer resistance at the anode and cathode for Fe$_2$O$_3$ dissociation	I_i^{MgO}	ionic current for MgO dissociation
$R_{ct(a,c)}^{MgO}$	charge transfer resistance at the anode and cathode for MgO dissociation	$I_i^{ZrO_2}$	ionic current for ZrO$_2$ dissociation
$R_{ct(a,c)}^{ZrO_2}$	charge transfer resistance at the anode and cathode for ZrO$_2$ dissociation	$I_{e(YSZ)}$	electronic current passing the YSZ membrane
$R_{e(YSZ)}$	electronic resistance of the YSZ membrane	I_T	total current
$R_{e(flux)}$	electronic resistance of the flux between YSZ and bubbling tube		

$$i = 2FA_c J_{MgO,flux/cathode} =$$
$$-2FA_c D_{MgO(flux)} \frac{C_{MgO(flux)}^{(i)} - C_{MgO(flux)}^0}{\delta_c}, \qquad [12]$$

where A_c is the effective cathode's area for the electrochemical half-cell reaction: $Mg^{2+} + 2e^- \rightarrow Mg(g)$.

The largest rate of mass transport of MgO occurs when $C_{MgO(flux)}^{(i)} = 0$. The value of the current under this condition is called the cathodic limiting current, $i_{l,c}$, where

$$i_{l,c} = 2FA_c D_{MgO(flux)} \frac{C_{MgO(flux)}^0}{\delta_c} \qquad [13]$$

Solving Eqs. [10] through [13], $\eta_{conc,c}$ can be expressed as follows:

$$\eta_{conc,c} = \frac{RT}{2F} \ln\left(\frac{i_{l,c}}{i_{l,c} - i}\right) \qquad [14]$$

5. Anodic overpotential for O₂ evolution, $\eta_{over,anode/YSZ}$

The liquid silver anode is saturated with oxygen as it is in equilibrium with the oxygen in the air environment. At the liquid silver anode/YSZ interface, oxygen is produced when the applied potential exceeds the electric potential for MgO dissociation. Oxygen is injected from the YSZ membrane to the liquid silver, and the oxygen partial pressure at the liquid silver anode/YSZ interface reaches 1 atm, equal to the air pressure above the liquid silver. The diffusion of oxygen is slow because the liquid silver is not stirred. In order for the oxygen to form bubbles and leave the liquid silver, the oxygen partial pressure at the liquid silver anode/YSZ interface must exceed 1 atm. This difference in oxygen partial pressure generates an overpotential that must be exceeded to form oxygen bubbles. The overpotential for oxygen gas evolution is expressed as follows:

$$\eta_{over,anode/YSZ} = \frac{RT}{2F} \ln\left(\frac{a_{O_2(Ag)}^b}{a_{O_2(Ag)}^{(i)}}\right) = \frac{RT}{2F} \ln\left(\frac{P_{O_2(Ag)}^b}{P_{O_2(Ag)}^{(i)}}\right)$$
$$= \frac{RT}{2F} \ln\left(\frac{P_{O_2(Ag)}^b}{1 \text{ atm}}\right), \qquad [15]$$

where $a_{O_2(Ag)}^b$ and $P_{O_2(Ag)}^b$ are the oxygen activity and the oxygen partial pressure required for bubble formation at the liquid silver anode/YSZ interface, respectively; $a_{O_2(Ag)}^{(i)}$ and $P_{O_2(Ag)}^{(i)}$ are the oxygen activity and the oxygen partial pressure at the liquid silver anode/YSZ interface, respectively. Because the oxygen evolved forms bubbles at liquid silver anode/YSZ interface and leaves the liquid silver, there is negligible concentration polarization ($\eta_{conc,a}$) caused by oxygen atom's diffusion in the liquid silver anode. The increasing applied current increases the O₂ evolution rate, but does not affect the oxygen partial pressure for bubble formation at the anode/YSZ interface.

6. Current–potential relationship in polarization model

The general relationship between the applied voltage and the cell current for SOM electrolysis is obtained by substituting Eqs. [6], [8], [14], and [15] into [4]:

$$E_{applied} = \left| E_N^{MgO} \right| + i R_{ohm}$$
$$+ \frac{RT}{F} \ln \left[\left(\frac{i}{2i_0} \right) + \sqrt{\left(\frac{i}{2i_0} \right)^2 + 1} \right] \quad [16]$$
$$+ \frac{RT}{2F} \ln \left(\frac{i_{l,c}}{i_{l,c} - i} \right) + \frac{RT}{2F} \ln \left(\frac{P_{O_2(Ag)}^b}{1 \text{ atm}} \right)$$

The current–potential curve obtained from PDS measurement can be modeled using Eq. [16] to determine various polarization losses and quantify the unknown parameters, such as the exchange current, the cathodic limiting current, and the oxygen partial pressure required for bubble formation at the anode/YSZ interface.

7. Curve-fitting of the measured current–potential characteristics

The current–potential curve obtained from the PDS after the pre-electrolysis (the dashed line shown in Figure 3) can be modeled as per the polarization model (Eq. [16]).

The electric potential for MgO dissociation ($|E_N^{MgO}|$) producing Mg vapor at the cathode and O_2 at the anode was identified to be 2.08 V, less than $E_N^{0,MgO}$ (2.31 V). The explanation for the reduced potential was because the Ar bubbling through the cathode tube decreased $a_{Mg(g),c}$.[20] It is believed that the current observed before reaching 2.08 V is due to MgO dissociation resulting in the dissolution of Mg into the flux as per the reaction: MgO = Mg(flux) + 1/2 O_2(g). The current at 2.08 V can be used as the baseline for the curve-fitting. The difference between the measured current and the baseline current in the potential ranging from 2.08 V to 3.32 V is referred to as the net current. The ohmic resistance of the SOM cell (R_{ohm}) was measured to be 0.54 Ω (see Figure 2).

Mass-transfer-limited behavior was not observed (see the PDS after pre-electrolysis in Figure 3). Consequently, the anodic and the cathodic concentration polarizations can be ignored. Equation [16] can be written as follows:

$$E_{applied} = \left| E_N^{MgO} \right| + i R_{ohm}$$
$$+ \frac{RT}{F} \ln \left[\left(\frac{i}{2i_0} \right) + \sqrt{\left(\frac{i}{2i_0} \right)^2 + 1} \right] \quad [17]$$
$$+ \frac{RT}{2F} \ln \left(\frac{P_{O_2(Ag)}^b}{1 \text{ atm}} \right)$$

The experimental data of the applied potential and the net current were curved fitted into Eq. [17]. The exchange current, i_0, and the oxygen partial pressure for bubble formation at the anode/YSZ interface, $P_{O_2(Ag)}^b$, were treated as the fitting parameters, and the results are shown
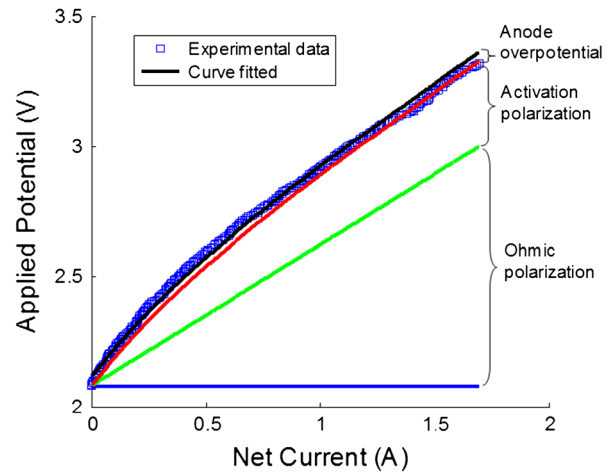
Fig. 9—The ohmic overpotential and the activation polarization as a function of the net current by modeling on the SOM electrolysis cell (Color figure online).

in Figure 9. The good match between the experimental data and the fitted curves justify the assumption that the concentration polarizations are negligible. The exchange current obtained from the curve fitting was 0.1154 A. Prior studies have shown that the charge transfer reaction at the interface between liquid metal electrode and the YSZ electrolyte is very fast.[31–33] Therefore, the exchange current value is believed to be limited by the cathodic material's structure and surface roughness, the concentration of MgO at the cathodic surface, etc. The charge transfer resistance at the cathode for MgO dissociation ($R_{ct,c}^{MgO}$) can be evaluated from the polarization model. $R_{ct,c}^{MgO}$ is the differential of the activation polarization (η_{act}) with respect to the ionic current for MgO dissociation (I_i^{MgO}), as expressed by Eq. [18].[34]

$$R_{ct,c}^{MgO} = \frac{d\eta_{act}}{di} \Big|_{i=I_i^{MgO}} = \frac{RT}{F} \frac{1}{\sqrt{\left(I_i^{MgO} \right)^2 + (2i_0)^2}} \quad [18]$$

When the electrolysis cell is at equilibrium ($I_i^{MgO} = 0$), $R_{ct,c}^{MgO}$ is given as Eq. [19], and it is equal to 0.531 Ω.

$$R_{ct,c}^{MgO} = \frac{d\eta_{act}}{di} \Big|_{i=0} = \frac{RT}{2Fi_0} \quad [19]$$

The oxygen partial pressure for bubble formation at the anode/YSZ interface, $P_{O_2(Ag)}^b$, obtained from the curve fitting was 1.747 atm. The O_2 bubble radius (r) was calculated to be 17.6 μm using the following equation[35]:

$$P_{O_2(Ag)}^b - P_{Ag}^{out} = \frac{2\sigma}{r}, \quad [20]$$

where $P_{Ag}^{out} = 1$ atm is the hydrostatic pressure outside O_2 bubble in liquid silver, and $\sigma = 658 \times 10^{-3}$ N/m is the surface tension of liquid silver at the oxygen partial

pressure of 1 atm at 1423 K (1150 °C).[36] It is to be noted that as O_2 bubble rises through the liquid silver, the pressure inside the oxygen bubble decreases, and therefore the volume of O_2 bubble increases. In addition, the volume of oxygen bubble might also increase due to multiple oxygen bubbles coalescing and merging.

Based on the curve fitting results, the ohmic polarization and the activation polarization were calculated as a function of current, and the results are also shown in Figure 9. In the current ranging from 1 to 1.7 A, the contributions from ohmic resistance and the charge transfer resistance to the total polarization were ~70 and ~30 pct, respectively; the contribution from the anodic overpotential for O_2 gas evolution (0.0342 V) is much smaller. The ohmic polarization was therefore dominating the total polarization in this current regime. This indicated that the performance of the SOM electrolysis can be improved by reducing the ohmic resistance, which can be realized by decreasing the thickness of the electrolyte (the YSZ membrane and the flux). The concentration polarizations were insignificant in the current ranging from 0 to 1.7 A. However, if the current continues to increase and approach the cathodic limiting current, then the contribution from the cathodic concentration polarization to the total polarization would become non-negligible. In that case, the cathodic concentration polarization should be considered in the modeling.

C. Maximum Allowable Applied Potential

As SOM electrolysis continues, more Mg dissolves into the flux, and thus the electronic conductivity of the flux increases. The dissolved Mg provides a pathway for the electronic current in the flux. There are both electronic and ionic currents passing through the flux and the YSZ membrane (see the equivalent circuit in Figure 8). As previously described, the increased electronic conductivity of the flux decreased the electronic potential drop across the flux and increased the potential drop across the YSZ membrane when a constant DC electric potential is applied across the entire cell. To avoid ZrO_2 dissociation, the potential drop across the YSZ membrane ($I_{e(YSZ)} \cdot R_{e(YSZ)}$) should not exceed the electric potential for ZrO_2 dissociation,

Fig. 10—The simplified equivalent circuit for SOM process when the applied potential is the maximum allowable applied potential, E_{MAAP}.

which is also the absolute value of the Nernst potential for ZrO_2 dissociation, $\left| E_N^{ZrO_2} \right|$. When the potential drop across the YSZ membrane is equal to $\left| E_N^{ZrO_2} \right|$, as expressed by Eq. [21], the ionic current for ZrO_2 dissociation, $I_i^{ZrO_2}$ becomes zero. In this case, the applied potential is defined as the maximum allowable applied potential (E_{MAAP}) to avoid ZrO_2 dissociation.

$$I_{e(YSZ)} \cdot R_{e(YSZ)} = \left| E_N^{ZrO_2} \right| \quad [21]$$

1. Analysis of simplified equivalent circuit

To calculate E_{MAAP}, it is necessary to simplify the equivalent circuit in Figure 8. According to the polarization model, the mass transfer resistances for MgO dissociation are negligible at the current ranging from 0 to 1.7 A. At the point when Mg dissolves in the flux and imparts electronic conductivity to the flux, the entire Fe_2O_3 must have already been removed. Therefore, the circuit branch for Fe_2O_3 dissociation can be eliminated. In addition, resistance of external lead wires (R_{ex}) was negligible. The simplified equivalent circuit is shown in Figure 10.

According to the Kirchhoff's Current Law (KCL),

$$I_T = I_i^{MgO} + I_{e(YSZ)} \quad [22]$$

The Kirchhoff's Voltage Law applied to the closed circuits in the simplified equivalent circuit gives

$$E_{MAAP} = I_T \cdot R_{cc} + I_{e(YSZ)} \cdot \left(R_{e(YSZ)} + R_{e(flux)} \right) \quad [23]$$

$$E_{MAAP} = I_T \cdot R_{cc} + I_i^{MgO} \cdot \left(R_{i(YSZ)}^{MgO} + R_{i(flux)}^{MgO} + R_{ct,c}^{MgO} \right) + \left| E_N^{MgO} \right| \quad [24]$$

Equations [21] through [24] are independent, and they form a system of equations in the four unknown parameters $I_{e(YSZ)}$, I_T, I_i^{MgO}, and E_{MAAP}. When the applied potential is E_{MAAP}, the current efficiency (CE) can be represented as

$$CE = \frac{I_i^{MgO}}{I_T} \quad [25]$$

2. Quantification of E_{MAAP}

To quantify E_{MAAP} for the SOM experiment described in this article, the values of the parameters ($\left| E_N^{ZrO_2} \right|$, R_{cc}, $R_{i(YSZ)}^{MgO}$, $R_{i(flux)}^{MgO}$, $R_{e(flux)}$, and $R_{e(YSZ)}$) in the system of equations need to be either measured during the experiment or calculated based on the available literature data. $\left| E_N^{ZrO_2} \right|$ can be calculated according to the Nernst equation as follows:

$$E_N^{ZrO_2} = E_N^{0,ZrO_2} + \frac{RT}{4F} \ln \left(\frac{a_{ZrO_2(s)}}{a_{Zr(s)} \, a_{O_2(g),anode/YSZ}} \right), \quad [26]$$

where $E_N^{0,ZrO_2} = -2.153\,V$ is the standard Nernst potential for ZrO_2 dissociation at $T = 1423$ K (1150 °C)[37]; $a_{ZrO_2(s)}$ and $a_{Zr(s)}$ are the activities of the solid ZrO_2 and
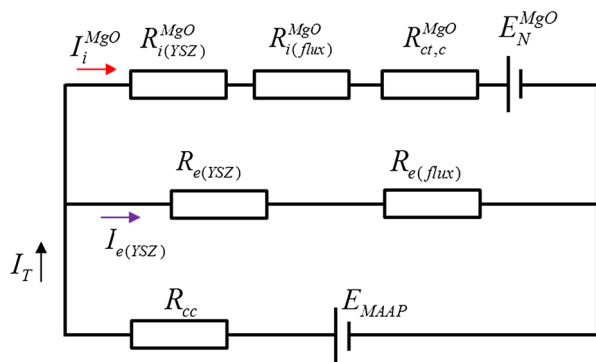
Table III. Values Used to Calculate the Unknown Parameters ($I_{e(YSZ)}$, I_T, I_i^{MgO}, and E_{MAAP})

Category	Description	Value
Trial value	electronic resistance of YSZ Membrane ($R_{e(YSZ)}$)	10 Ω, 50 Ω, and 100 Ω
Calculated parameters	ionic resistance of YSZ membrane ($R_{i(YSZ)}$)	0.071 Ω
	resistance of the anode current collector (R_{cc})	0.125 Ω
	ionic resistance of the flux ($R_{i(flux)}^{MgO}$) between the bubbling tube and the YSZ membrane	0.344 Ω
Measured parameters	potential for ZrO_2 dissociation ($|E_N^{ZrO_2}|$)	2.17 V
	potential for MgO dissociation producing magnesium vapor at the cathode ($|E_N^{MgO}|$)	2.08 V
	electronic resistance of the flux ($R_{e(flux)}$) between the bubbling tube and the YSZ membrane	12.397 Ω (1st), 6.823 Ω (2nd), 1.806 Ω (3rd), 2.386 Ω (4th)

Zr at the cathode side of the YSZ membrane, and they are both equal to unity; and $a_{O_2(g),anode/YSZ}$ is the activity of oxygen bubble at the anode/YSZ interface, and it is equal to 1.747. Therefore, $|E_N^{ZrO_2}|$ is equal to 2.17 V.

The ohmic resistance of the LSM-Inconel current collector has been reported to be approximately 0.125 Ω at 1423 K (1150 °C) in earlier experiments.[6] Because of similar cell constants, the ohmic resistance of the LSM-Inconel current collector used in this SOM experiment (R_{cc}) is estimated to be 0.125 Ω.

The ionic resistance of the YSZ membrane ($R_{i(YSZ)}$) depends on the ionic conductivity ($\sigma_{i(YSZ)}$), the cross-sectional area ($A(x)$), and the thickness of the YSZ membrane (L_{YSZ}) as shown in Eq. [27].

$$R_{i(YSZ)} = \int_0^{L_{YSZ}} \frac{1}{\sigma_{i(YSZ)}} \frac{dx}{A(x)} \qquad [27]$$

Filal et al.[38] have reported the ionic conductivities of the YSZ membrane with different amounts of Y_2O_3 (3 and 9.5 mol pct). In this work, 6 mol pct YSZ membrane was employed, and its ionic conductivity at 1423 K (1150 °C) is estimated to be 21.88 S/m by interpolation from the literature data. The ionic resistance of the YSZ membrane is calculated to be 0.071 Ω.

The cell ohmic resistance was measured to be 0.54 Ω at the beginning of the experiment. No Mg was dissolved in the flux yet, and so the electronic resistances of the YSZ membrane and the flux were much higher than their ionic resistances. The contact resistance associated with all the interfaces and the ohmic resistances of the external lead wires are assumed to be negligible. Therefore, the ionic resistance of the flux between the bubbling tube and the YSZ membrane ($R_{i(flux)}^{MgO}$) is calculated to be 0.344 Ω by subtracting $R_{i(YSZ)}$ (0.071 Ω) and R_{cc} (0.125 Ω) from R_{ohm} (0.54 Ω). The value of $R_{i(flux)}^{MgO}$ was expected to be stable during the experiment because MgO concentration change in the flux was negligibly small.

To calculate the electronic resistance of the flux ($R_{e(flux)}$) between the bubbling tube and the YSZ membrane, Eq. [3] can be rearranged into Eq. [28] to write $R_{e(flux)}$ as a function of $R_{i(flux)}^{MgO}$ and $t_{e(flux)}$.

$$R_{e(flux)} = R_{i(flux)}^{MgO} \left(\frac{1}{t_{e(flux)}} - 1 \right) \qquad [28]$$

As the flux was stirred by bubbling gas, $t_{e(flux)}$ between the bubbling tube and the YSZ membrane is equal to $t_{e(flux)}$ between the bubbling tube and the reaction chamber (see Table II). Therefore, $R_{e(flux)}$ between the bubbling tube and the YSZ membrane can be calculated and the values are listed in Table III.

The electronic resistance of the YSZ membrane ($R_{e(YSZ)}$) depends on the electronic conductivity ($\sigma_{e,YSZ}$), $A(x)$, and L_{YSZ} as shown in the following equation:

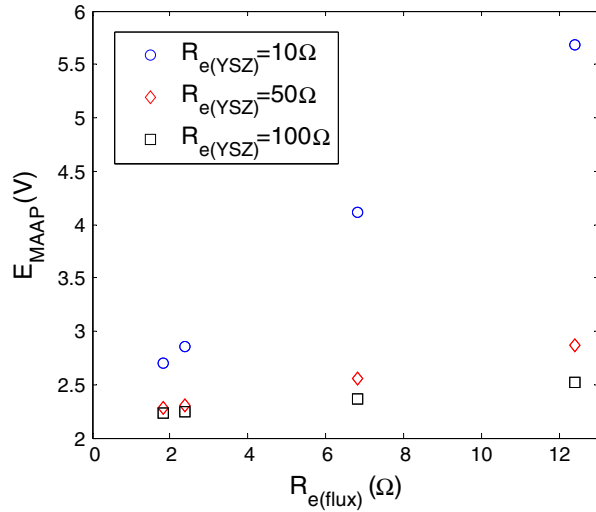$$R_{e(YSZ)} = \int_0^{L_{YSZ}} \frac{1}{\sigma_{e(YSZ)}} \frac{dx}{A(x)} \qquad [29]$$

Fig. 11—The calculated E_{MAAP} as a function of $R_{e(flux)}$ for different values of $R_{e(YSZ)}$.

Fig. 13—The calculated ionic current for MgO dissociation (I_i^{MgO}) as a function of $R_{e(flux)}$ for different values of $R_{e(YSZ)}$ when the applied potential is E_{MAAP}.

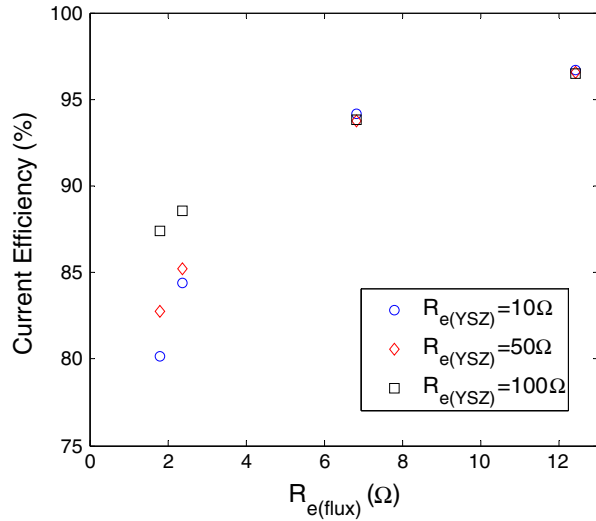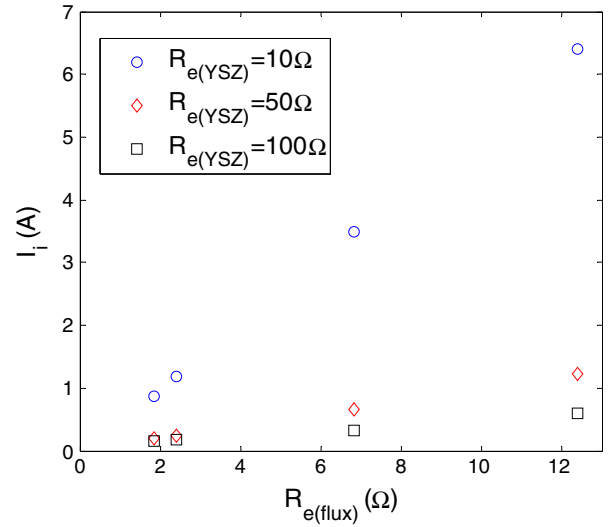Fig. 12—The calculated current efficiency as a function of $R_{e(flux)}$ for different values of $R_{e(YSZ)}$ when the applied potential is E_{MAAP}.

Park et al.[27] has reported that $\sigma_{e,YSZ}$ depends on the oxygen partial pressure distribution in the YSZ membrane. The oxygen partial pressure in the YSZ membrane during the SOM electrolysis is still ambiguous. Therefore, instead of calculating $R_{e(YSZ)}$, it is more realistic to take a series of trial values (10 Ω, 50 Ω, and 100 Ω) of $R_{e(YSZ)}$. The above trial values are chosen to obtain current efficiencies in the range that is experimentally observed (from 75 to 95 pct) and also the ionic currents for MgO dissociation when the applied potential is E_{MAAP}. The values of the parameters used to calculate the unknown parameters ($I_{e(YSZ)}$, I_T, I_i^{MgO}, and E_{MAAP}) are given in Table III.

Figure 11 shows the calculated E_{MAAP} as a function of $R_{e(flux)}$ for different values of $R_{e(YSZ)}$. The calculated E_{MAAP} decreases as $R_{e(flux)}$ decreases for each value of $R_{e(YSZ)}$. As more Mg dissolves into the flux,

$R_{e(flux)}$ becomes smaller, and thus E_{MAAP} becomes smaller as well. During the SOM experiment, $R_{e(flux)}$ can be monitored, and applied potential can be adjusted accordingly to avoid ZrO_2 dissociation. In addition, E_{MAAP} can be increased by increasing $R_{e(flux)}$. This can be accomplished by operating the SOM electrolysis cell at low total pressures which is an effective method of removing Mg dissolved in the flux and reducing the electronic conductivity of the flux.[20] Figure 11 also shows that the calculated E_{MAAP} increases as $R_{e(YSZ)}$ decreases for each value of $R_{e(flux)}$. It suggests that E_{MAAP} can be increased by decreasing $R_{e(YSZ)}$. This can be realized by reducing the thickness of the YSZ membrane and/or increasing the cross-sectional area of the YSZ membrane. Another method is to make the YSZ membrane more mixed conducting or to employ a different mixed-conducting membrane that conducts both oxygen ions and electrons.

Figure 12 shows the calculated current efficiency as a function of $R_{e(flux)}$ for different values of $R_{e(YSZ)}$ when the applied potential is E_{MAAP}. It should be noted that in this modeling the applied potential (E_{MAAP}) varies with both $R_{e(flux)}$ and $R_{e(YSZ)}$ (see Figure 11). For same $R_{e(YSZ)}$, the calculated current efficiency decreases as $R_{e(flux)}$ decreases, consistent with the experimental results in this work. Figure 12 also shows that when $R_{e(flux)}$ is greater than 6 Ω, the current efficiency is independent of $R_{e(YSZ)}$. When $R_{e(YSZ)}$ is small, the current efficiency increases with the increasing $R_{e(YSZ)}$. This is because the electronic current in the flux is blocked by the YSZ membrane. Therefore, $R_{e(YSZ)}$ cannot be too small in order to maintain a high current efficiency of the SOM electrolysis process.

In addition to current efficiency, the performance of the SOM electrolysis can also be evaluated by the production rates of Mg and O_2, which are linearly proportional to the ionic current for MgO dissociation (I_i^{MgO}). Figure 13 shows the calculated I_i^{MgO} as a function of $R_{e(flux)}$ for different values of $R_{e(YSZ)}$ when the applied potential is

E_{MAAP}. The dependence of I_i^{MgO} on $R_{\text{e(flux)}}$ and $R_{\text{e(YSZ)}}$, is similar to that of E_{MAAP}. A high $R_{\text{e(flux)}}$ and a low $R_{\text{e(YSZ)}}$ allow for a high E_{MAAP}, and thus a high I_i^{MgO} according to the simplified equivalent circuit in Figure 10.

Overall, a high $R_{\text{e(flux)}}$ and a relatively low $R_{\text{e(YSZ)}}$ are required to achieve ZrO_2 stability, high current efficiency, and high production rate of Mg and O_2.

V. CONCLUSIONS

SOM electrolysis experiment was successfully performed in producing Mg at the cathode and O_2 at the anode. Dissolved Mg metal was responsible for imparting electronic conductivity to the flux. An inverse correlation between the electronic transference number of the flux and the current efficiency of the SOM electrolysis was observed. Based on the experimental results, a new equivalent circuit of the SOM electrolysis process was presented by taking into account the dissociations of Fe_2O_3, MgO, and ZrO_2, and the impact of the electronic conductivity in the flux. In addition, a polarization model for Mg and O_2 production was developed to analyze various polarization losses. The maximum allowable applied potential (E_{MAAP}) to avoid ZrO_2 dissociation was quantified as a function of the electronic resistance of the flux ($R_{\text{e(flux)}}$) for different values of electronic resistance of the YSZ membrane ($R_{\text{e(YSZ)}}$). A high $R_{\text{e(flux)}}$ and a relatively low $R_{\text{e(YSZ)}}$ are required to achieve ZrO_2 stability, high current efficiency, and high production rates of Mg and O_2.

REFERENCES

1. U.B. Pal, D.E. Woolley, and G.B. Kenney: *JOM*, 2001, vol. 53 (10), pp. 32–35.
2. A. Krishnan, U.B. Pal, and X.G. Lu: *Metall. Mater. Trans. B*, 2005, vol. 36B, pp. 463–73.
3. U.B. Pal and A.C. Powell: *JOM*, 2007, vol. 59 (5), pp. 44–49.
4. X. Guan, P.A. Zink, U.B. Pal, and A.C. Powell: *Metall. Mater. Trans. B*, 2013, vol. 44B, pp. 261–71.
5. X. Guan, U.B. Pal, and A.C. Powell: *JOM*, 2013, vol. 65 (10), pp. 1285–92.
6. X. Guan, U.B. Pal, S. Gopalan, and A.C. Powell: *J. Electrochem. Soc.*, 2013, vol. 160 (11), pp. F1179–86.
7. S. Das: *JOM*, 2008, vol. 60 (11), pp. 63–69.
8. M. Suput, R. Delucas, S. Pati, G. Ye, U. Pal, and A.C. Powell, IV: *Miner. Process. Extr. Metall.*, 2008, vol. 117 (2), pp. 118–22.
9. A. Krishnan, X.G. Lu, and U.B. Pal: *Scand. J. Metall.*, 2005, vol. 34 (5), pp. 293–301.
10. S. Pati, R. Delucas, and U.B. Pal: in *EPD Congress 2008*, S.M. Howard, ed., TMS, Warrendale, PA, 2008, pp. 121–26.
11. Y. Jiang, P.A. Zink, and U.B. Pal: *ECS Trans.*, 2012, vol. 41 (33), pp. 171–80.
12. Y. Jiang, J. Xu, X. Guan, U.B. Pal, and S.N. Basu: *MRS Proc.*, 2013, vol. 1493, pp. 231–35.
13. A. Roan, S. Pati, S.N. Basu, and U.B. Pal: *TMS Supplemental Proceeding, Vol. 1: Materials Processing and Energy Materials*, Wiley, New Jersey, 2011, pp. 717–21.
14. X. Lu, X. Zou, C. Li, Q. Zhong, W. Ding, and Z. Zhou: *Metall. Mater. Trans. B*, 2012, vol. 43B, pp. 503–12.
15. B. Zhao, X. Lu, Q. Zhong, C. Li, and S. Chen: *Electrochim. Acta*, 2010, vol. 55 (8), pp. 2996–3001.
16. X. Zou, X. Lu, C. Li, and Z. Zhou: *Electrochim. Acta*, 2010, vol. 55 (18), pp. 5173–79.
17. X. Zou, X. Lu, Z. Zhou, C. Li, and W. Ding: *Electrochim. Acta*, 2011, vol. 56 (24), pp. 8430–37.
18. E. Gratz, S. Pati, J. Milshtein, A. Powell, and U. Pal: *Electrometallurgy 2012 (TMS)*, M.L. Free, M. Moats, G. Houlachi, E. Asselin, A. Allanore, J. Yurko, and S. Wang, eds., Wiley, New Jersey, 2012, pp. 111–18.
19. A. Dworkin and M. Bredig: *J. Phys. Chem.*, 1971, vol. 75 (15), pp. 2340–44.
20. E. Gratz: Ph.D. Dissertation, Boston University, 2013.
21. E.S. Gratz, J.D. Milshtein, and U.B. Pal: *J. Am. Ceram. Soc.*, 2013, vol. 96 (10), pp. 3279–85.
22. P. Chartrand and A.D. Pelton: *Metall. Mater. Trans. A*, 2001, vol. 32A, pp. 1385–96.
23. T.H. Etsell and S.N. Flengas: *Metall. Trans.*, 1971, vol. 2 (10), pp. 2829–32.
24. S.C. Britten and U.B. Pal: *Metall. Mater. Trans. B*, 2000, vol. 31B, pp. 733–53.
25. K.R. Copper and M. Smith: *J. Power Sources*, 2006, vol. 160, pp. 1088–95.
26. A.V. Virkar: *J. Power Sources*, 2005, vol. 147 (1–2), pp. 8–31.
27. J. Park and R.N. Blumenthal: *J. Electrochem. Soc.*, 1989, vol. 136 (10), pp. 2867–76.
28. S. Pati, K.J. Yoon, S. Gopalan, and U.B. Pal: *Metall. Mater. Trans. B*, 2009, vol. 40B, pp. 1041–53.
29. K.J. Yoon, P. Zink, S. Gopalan, and U.B. Pal: *J. Power Sources*, 2007, vol. 172 (1), pp. 39–49.
30. A.J. Bard and L.R. Faulkner: *Electrochemical Methods: Fundamentals and Applications*, 2nd ed., Wiley, New Jersey, 2001.
31. K.E. Oberg, L.M. Friedman, W.M. Boorstein, and R.A. Rapp: *Metall. Trans.*, 1973, vol. 4 (1), pp. 75–82.
32. S. Yuan, U. Pal, and K.C. Chou: *J. Electrochem. Soc.*, 1994, vol. 141 (2), pp. 467–74.
33. P. Soral, U. Pal, H.R. Larson, and B. Schroeder: *Metall. Mater. Trans. B*, 1999, vol. 30B, pp. 307–21.
34. K.J. Yoon: Ph.D. Dissertation, Boston University, 2008.
35. C.H.P. Lupis: *Chemical Thermodynamics of Materials*, Elsevier, Amsterdam, 1983.
36. S. Ozawa, K. Morohoshi, T. Hibiya, and H. Fukuyama: *J. Appl. Phys.*, 2010, vol. 107, p. 014910.
37. A. Roine: HSC Chemistry, 5.11, Outokumpu Research Oy, 2002.
38. M. Filal, C. Petot, M. Mokchah, C. Chateau, and J.L. Carpentier: *Solid State Ionics*, 1995, vol. 80, pp. 27–35.